ACS APPLIED MATERIALS & INTERFACES

Research Article

www.acsami.org

FITC Doped Rattle-Type Silica Colloidal Particle-Based Ratiometric Fluorescent Sensor for Biosensing and Imaging of Superoxide Anion

Ying Zhou,[†,∥] Jie Ding,[‡,†,∥] Tingxizi Liang,[†] E. S. Abdel-Halim,[§] Liping Jiang,*[,†] and Jun-Jie Zhu*[,†]

[†]State Key Laboratory of Analytical Chemistry for Life Science, Collaborative Innovation of Chemistry for Life Science, School of Chemistry and Chemical Engineering, Nanjing University, Nanjing 210093, P. R. China

[‡]Guangdong Provincial Key Laboratory of Medical Molecular Diagnostics, China-America Cancer Research Institute, Guangdong Medical University, Dongguan 523808, P. R. China

[§]Chemistry Department, College of Science, King Saud University, Riyadh 11451, P.O. Box 2455, Kingdom Saudi Arabia

Supporting Information

ABSTRACT: Fluorescent nanosensors have been widely applied in recognition and imaging of bioactive small molecules; however, the complicated surface modification process and background interference limit their applications in practical biological samples. Here, a simple, universal method was developed for ratiometric fluorescent determination of general small molecules. Taking superoxide anion ($O_2^{\bullet-}$) as an example, the designed sensor was composed of three main moieties: probe carrier, rattle-type silica colloidal particles ($mSiO_2$@$hmSiO_2$ NPs); reference fluorophore doped into the core of NPs, fluorescein isothiocyanate (FITC); fluorescent probe for superoxide anion, hydroethidine (HE). In the absence of $O_2^{\bullet-}$, the sensor just emitted green fluorescence of FITC at 518 nm. When released HE was oxidized by $O_2^{\bullet-}$, the oxidation product exhibited red fluorescence at 570 nm and the intensity was linearly associated with the concentration of $O_2^{\bullet-}$, while that of reference element remained constant. Accordingly, ratiometric determination of $O_2^{\bullet-}$ was sensitively and selectively achieved with a linear range of 0.2−20 μM, and the detection limit was calculated as low as 80 nM. Besides, the technique was also successfully applied for dual-emission imaging of $O_2^{\bullet-}$ in live cells and realized visual recognition with obvious fluorescence color change in normal conditions or under oxidative stress. As long as appropriate reference dyes and sensing probes are selected, ratiometric biosensing and imaging of bioactive small molecules would be achieved. Therefore, the design could provide a simple, accurate, universal platform for biological applications.

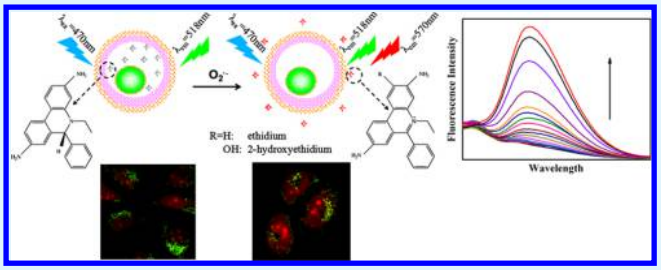

KEYWORDS: *FITC@$mSiO_2$@$hmSiO_2$, hydroethidine, bioactive small molecules, superoxide anion, ratiometric fluorescent sensor*

INTRODUCTION

Presently, bioactive small molecules have attracted extensive attention due to their roles in biological processes, such as signaling molecules, biological tools, or therapeutic drugs.[1,2] For example, the reactive oxygen species (ROS) are important cellular signaling species and inevitable products of the aerobic metabolism in cells, which could help to inhibit the breeding of bacterial and fungal pathogens.[3] But the overproduction of ROS would lead to the so-called oxidative stress and cause some diseases, such as cancers, cardiovascular diseases, and neurodegenerative diseases.[4,5] Superoxide anion ($O_2^{\bullet-}$) is a primary species of ROS, which has highly oxidative activity. Excessive accumulation of $O_2^{\bullet-}$ in cells can cause oxidative damage to proteins, DNA, and liposomes, even inducing cell death.[6] Therefore, biosensing and bioimaging of bioactive small molecules is of great importance to the early diagnosis and prevention of related diseases. Although many fluorescent nanosensors with good temporal and spatial resolution have been successfully designed and applied in biological samples, challenges still remain in their feasibility and efficiency.[7,8] In many cases, nanosensors suffer from errors in background interference and complexity in surface modification.[9−11] So, a simple, universal, and sensitive detection method is urgently expected. As noted above, superoxide anion operates as an important cellular signaling molecule in the physiological or pathological conditions. Therefore, in this paper, the detection of $O_2^{\bullet-}$ is taken as an example to demonstrate a universal method for sensing bioactive small molecules like ROS.

To design an excellent nanosensor, we choose the rattle-type silica colloidal particles as nanocarriers. Rattle-type structures are a special type of core−shell structures and usually made up of three different components, namely core, void, and shell. Compared with conventional nanoparticles, the hollow silica shows good biocompatibility, high stability, and excellent drug loading efficiency, which ensures it to be an ideal nanocarrier.[12,13] Thus, $O_2^{\bullet-}$ fluorescent probes could be loaded in

Received: January 26, 2016
Accepted: February 24, 2016
Published: February 24, 2016

DOI: 10.1021/acsami.6b01031
ACS Appl. Mater. Interfaces 2016, 8, 6423−6430

the hollow structure to form $O_2^{\bullet-}$ nanosensor. Currently, $O_2^{\bullet-}$ fluorescent probes with high sensitivity and selectivity have been well developed and even some commercialized probes are available, which can provide rapid response and visual identification to $O_2^{\bullet-}$ in cells. For this reason, many scientists have used fluorescent probes for the detection and imaging of $O_2^{\bullet-}$ in cells.[14−16] However, some limitations still exist in these single emission intensity-based probes, such as influences of probe concentration and excitation intensity, errors from detection environment.[17] Fortunately, ratiometric fluorescent probes can overcome the limitation of intensity-based fluorescent probes because they usually obtain two emission peaks on the same excitation wavelength and the ratio of the two fluorescence intensities can eliminate the interference from probe concentration, excitation light source, and background fluorescence.[18−20] Thus, we prefer to design a highly selective and sensitive ratiometric fluorescent sensor to detect $O_2^{\bullet-}$ in cells. Due to the special structure of rattle-type silica colloidal particles, some fluorescent small molecules could be doped into the silica core, which could serve as a reference element for the fluorescence signal molecule. Moreover, the dye-doped silica NPs can get increased photostability and lower toxicity than pure dye molecules.[21] At present, fluorescein isothiocyanate (FITC) is the most widely used fluorophore with a narrow emission at 518 nm (excited at 470 nm).[22] On the one hand, the emission of FITC is well separated from the emission of oxidation products of hydroethidine (HE), a specific fluorescent probe toward $O_2^{\bullet-}$.[9,23] On the other hand, its absorption spectrum has appropriate overlap with that of HE oxidation products. Thus, they could be excited at the same wavelength (470 nm) and obtain a separated emission peak. Here, FITC is doped into the core of rattle-type silica to form hollow silica nanoparticles with green fluorescence (FITC@$mSiO_2$@$hmSiO_2$), which could be used as the carrier and reference fluorophore for $O_2^{\bullet-}$ probe (HE).

Herein, we developed a novel ratiometric fluorescent nanosensor for the biosensing and imaging of $O_2^{\bullet-}$ in cells. As shown in Scheme 1, the nanosensor was composed of two components: FITC@$mSiO_2$@$hmSiO_2$ nanoparticles (FMH NPs) as the reference signal element and probe carrier; nonfluorescent HE as the probe for $O_2^{\bullet-}$. Upon excitation at 470 nm, the emission peaks of FMH NPs and the oxidation product of HE were located at 518 and 570 nm, respectively. When the nanosensor was mixed with $O_2^{\bullet-}$, the fluorescence intensity of HE oxidation products was gradually enhanced with the increased concentration of $O_2^{\bullet-}$, while the fluorescence intensity of FMH NPs remained constant. By comparing the ratio between the integrated intensity of FMH NPs and HE oxidation products, we could draw a conclusion that the detection range of the nanosensor to $O_2^{\bullet-}$ was 0.2−20 μM and the detection limit was calculated as low as 80 nM. Compared with other sensors, the nanosensor has three main advantages: first, the rattle-structure silica colloidal particle could dope fluorescent dye into the core and load fluorescent probe in the hollow structure, forming an excellent ratiometric fluorescent nanosensor, which is simple and universal; second, the enhanced permeability and retention (EPR) effect could help the nanosensor to enter the cells, increasing the concentration of probe in cells; third, the dual-emission sensor could eliminate background interference and improve the accuracy of the method. Besides, upon changing the concentration of analytes, a clear color change of the overlay images could be easily observed in cells. Thus, the ratiometric fluorescent nanosensor provided an efficient and universal strategy for accurately and sensitively detecting bioactive small molecules in cells.

Scheme 1. Ratiometric Fluorescent Biosensing and Imaging of $O_2^{\bullet-}$ Based on the FMH NPs-HE Sensor

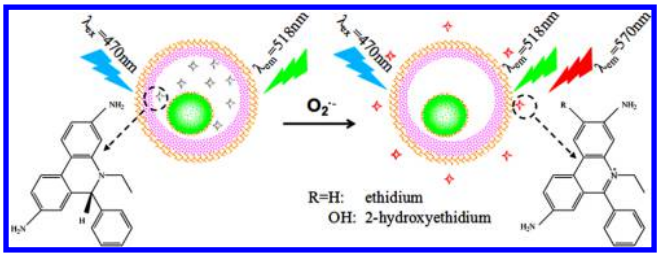

EXPERIMENTAL SECTION

Chemicals and Materials. Fluorescein isothiocyanate isomer I (FITC, ≥ 90%), tetraethyl orthosilicate (TEOS, 98%), (3-Aminopropyl) triethoxysilane (APTES, 98%), PVP (M_w ≈ 40 000), PVP (M_w ≈ 10 000), hydroethidine (HE, 95%), xanthine (X, 98%), xanthine oxidase from bovine milk (XO), and diethylamine NONOate sodium salt hydrate (DEA NONOate, ≥ 97%) were supplied by Sigma-Aldrich. Dimethyl sulfoxide (DMSO), $K_2HPO_4{\cdot}3H_2O$, KH_2PO_4, NaOH, KCl, NaCl, $FeCl_2{\cdot}4H_2O$, 2,2′-azobis(2-methylpropionamidine) dihydrochloride (AAPH), and NaClO were obtained from Sinopharm Chemical Reagent Co. Ltd. Glutathione (GSH), hydrogen peroxide (H_2O_2, 30%), $NaNO_2$ were purchased from Aladdin Chemistry Co. Ltd. CCK-8 kit was purchased from Dojindo Molecular Technologies, Inc. ROSup from reactive oxygen species (ROS) assay kit was obtained from Beyotime Institute of Biotechnology (Nantong, China). Ultrapure water made from a Milli-Q system (Millipore, U.S.A.), was used for all experiments. All reagents were used directly without further purification.

According to the previous studies, the enzymatic reaction of xanthine (X; 300 μM) and xanthine oxidase (XO; 0.01 U/mL) could generate 100 μM of $O_2^{\bullet-}$.[24−26] The reaction of HE with $O_2^{\bullet-}$, supplied by X/XO system in potassium phosphate buffer (PBS, 100 mM) at 25 °C, showed a time-dependent fluorescence increase and finished within 40 min (Figure S1). For interference assay, Fenton reaction (Fe^{2+}/H_2O_2 = 1:10) was used to generate hydroxyl radical. Hypochlorite ion (ClO^-) was produced by NaClO. The first singlet oxygen ($^1O_2$) was chemically provided by H_2O_2 and NaClO. Peroxynitrite ($ONOO^-$) stock solution was obtained by reaction of H_2O_2 with $NaNO_2$ in HCl at 0 °C and kept at −20 °C.[27] Decomposition of DEA NONOate was applied to produce nitric oxide (NO). Alkyl peroxyl radical ($ROO^{\bullet}$) was prepared from the thermolysis of AAPH at 37 °C.

Instrumentation. Transmission electron microscopy (TEM) images were measured on a JEM-1011 electron microscope (100 kV, JEOL). UV−vis spectra was obtained on a UV-3600 spectrophotometer (Shimadzu). Fluorescence intensity was recorded by a F-7000 Fluorescence Spectrometer (Hitachi). CCK-8 assay was measured using a Varioskan Flash microplate reader (ThermoFisher Scientific). Dynamic light scattering (DLS) was performed on BI-200SM Laser Light Scattering Instrument (Brookhaven). Confocal laser scanning microscopy (CLSM) images were obtained on a Leica TCS SP5 microscope. Flow cytometry experiments were taken on FC500 Cell Analyzer (Beckman).

Preparation of FITC@SiO_2. FITC and (3-aminopropyl) triethoxysilane (APTES) were mixed in ethanol solution and stirred overnight to prepare FITC-modified triethoxysilane. Then, FITC@SiO_2 nanoparticles were obtained by a modified Stöber method. 1.92 mL tetraethyl orthosilicate (TEOS) and 1 mL FITC-modified APTES (TEOS/FITC-APTES with a molar ratio of 20:1) were added into the mixture of 40 mL ethanol, 0.835 mL water, and 2.5 mL ammonia hydroxide aqueous solution (28 wt %). The mixture was stirred at 50

DOI: 10.1021/acsami.6b01031
ACS Appl. Mater. Interfaces 2016, 8, 6423−6430

°C for 6 h and then kept for additional 2 h at room temperature. The final product was centrifuged and washed with water for three times.

Preparation of FITC@mSiO$_2$@hmSiO$_2$. We prepared the rattle-type silica colloidal particles according to a "surface protected etching process". First, the as-prepared FITC@SiO$_2$ NPs were mixed with PVP (0.6 g, $M_w \approx 40\,000$) and stirred at room temperature. Five hours later, the particles were collected by centrifugation, washed with ethanol several times and redispersed in 10 mL ethanol. Next, 30 mL ethanol, 0.835 mL water, and 2.5 mL ammonia hydroxide aqueous solution (28 wt %) were mixed under intensive stirring. Then the FITC-SiO$_2$@PVP NPs and TEOS (3.84 mL) were added in turn and stirred for 3 h at room temperature. The products were collected by centrifugation and washed for several times with water to remove the residual ammonia hydroxide aqueous solution. Finally, they were dispersed in water and mixed with PVP (1.0 g, $M_w \approx 10\,000$) under stirring for 5 h at room temperature. Again, the products were centrifuged and washed with ethanol. After being dispersed in 40 mL water, NaOH aqueous solution (5 mL, 0.20 g/mL) was added to the system to initiate etching. After etching for a certain time, the resulting products were washed with water and ethanol several times, and finally dispersed in 10 mL deionized water.

In Vitro Probe Loading and Release. FITC@mSiO$_2$@hmSiO$_2$ was mixed with different concentrations of HE (in ethanol) and stirred for 24 h. Then, the nanosensors were collected by centrifugation and washed with PBS. For the probe release assay, 5 mg HE-loaded nanosensors were dispersed in 20 mL release medium and kept under stirring. Several hours later, the solution was centrifuged and the release medium (8 mL) was taken, followed by the addition of the same amount of fresh medium. The concentration of HE was measured by a UV−vis absorption wavelength at 265, 345 nm.[28] The loading amount of HE was calculated as follows: $(M_{Initial}\text{-}M_{Final})/M_{FMH\ NPs}$.

Cell Culture and CCK-8 Assay. HeLa cells were supplied by Nanjing KeyGen Biotech Co. Ltd. and cultured in growth medium containing Dulbecco's Modified Eagle Medium (DMEM), supplemented with 10% fetal bovine serum (v/v), penicillin (100 units/mL), streptomycin (100 μg/mL) at 37 °C in a 5% CO_2 incubator. CCK-8 assay was performed to measure cell viability. First, HeLa cells were seeded in 96-well plate at a density of 5000 cells per well and cultured for 24 h. Then, nanosensors (from 5 μg/mL to 500 μg/mL), dispersed in culture media, were added to wells. After 24 h of incubation, the media were removed, fresh media (100 μL) containing CCK-8 (10 μL) were added to each well and incubated for 2 h. When the color of the solution turned to orange, its absorbance was measured by a microplate reader at the wavelength of 450 nm. Relative cell viability was determined as follows: $(OD_{test}/OD_{control}) \times 100\%$. All the experiments were repeated at least 3 times.

In Vivo Fluorescence Imaging. HeLa cells (50 000 cells per dish) were seeded in a Petri dish for 24 h, and then nanosensors with the concentration of 200 μg/mL were added. After incubating for 12 h, the media were removed, and the cells were washed with PBS three times to remove the residual nanosensors. Then, fluorescence imaging in live cells were taken using a confocal laser scanning microscope under a 20× objective. Upon excitation at 488 nm, the fluorescent imaging of FMH NPs was obtained from a 500−535 nm channel, while that of HE oxidation products was collected from a 540−610 nm channel. For sensing the generated $O_2^{\bullet-}$ under oxidative stress, ROSup (50 mg/mL, 1 μL) was added. To verify the production of $O_2^{\bullet-}$, cells were treated with 2 mM GSH for 30 min before adding ROSup.

Flow Cytometry Analysis. To detect the fluorescence intensity of the dual-emissions in cells, flow cytometry experiments were taken. In detail, every well of 6-well plate was seeded with 150 000 HeLa cells, followed by culturing for 24 h. Then, 300 μg/mL sensor (2 mL) was added to each well and incubated for 12 h. After treatment with ROSup or GSH, cells were detached by trypsin, and then centrifuged and washed by PBS for several times. Finally, they were redispersed in PBS for determination.

RESULTS AND DISCUSSION

Characterization of FITC@SiO$_2$, FITC@mSiO$_2$@hmSiO$_2$, and FITC@mSiO$_2$@hmSiO$_2$@HE. In brief, the nanosensor was composed of a hollow silica structure (FMH NPs) and $O_2^{\bullet-}$ probe (HE). The synthetic procedure of FMH NPs was illustrated in Scheme 2. In order to dope FITC into the rattle-type silica nanoparticles, we first obtained FITC@SiO$_2$ NPs using a modified Stöber method.[29] FITC-modified triethoxysilane was obtained from the reaction between isothiocyanate group of FITC and the amino group of APTES, and then FITC@SiO$_2$ NPs was synthesized by adding suitable TEOS into the reacting system.[30] Next, FITC@SiO$_2$ NPs were used as cores to prepare FITC@mSiO$_2$@hmSiO$_2$ (FMH NPs) by "a surface-protected etching process".[31] In details, PVP with high molecular weight was fabricated on the surface of the core by hydrogen-bond interaction.[32] Then, another silica layer was deposited on the as-prepared particles by the Stöber method again, followed by the absorption of outer PVP layer with low molecular weight. Finally, the FITC@SiO$_2$@SiO$_2$ NPs was etched by NaOH solution and FITC@mSiO$_2$@hmSiO$_2$ NPs with core (FITC@mSiO$_2$ NP), hollow cavity, mesoporous silica shells were thus obtained (Figure 1a). This special structure resulted from the different protection efficacy of the PVP with different molecular weight.[31]

Scheme 2. Preparation of FITC@mSiO$_2$@hmSiO$_2$ and Sensor FMH NPs-HE

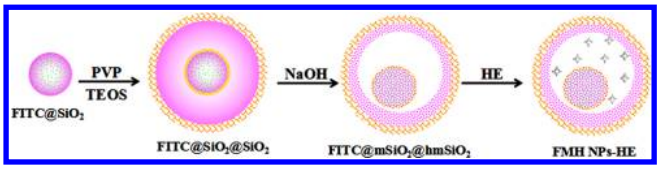

In Figure S2, the TEM image indicated that the average diameter of FITC@SiO$_2$ NPs was 80 nm, while the FMH NPs were dispersed with an average size of 120 nm (Figure 1a). The excellent dispersity of FMH NPs was also confirmed by dynamic light scattering measurements (Figure 1b). With the

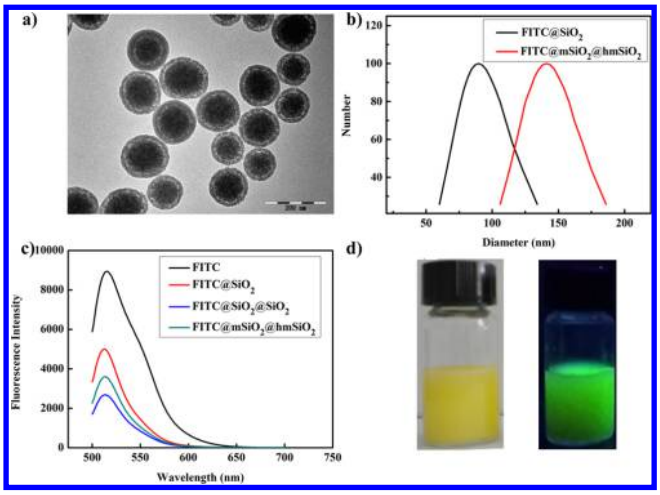

Figure 1. (a) TEM image of FMH NPs; (b) the hydrodynamic size distribution of FITC@SiO$_2$ and FMH NPs by DLS measurements; (c) fluorescence emission spectra of FITC, FITC@SiO$_2$, FITC@SiO$_2$@SiO$_2$, and FMH NPs (upon excitation at 470 nm); and (d) photographs of FMH NPs with or without UV excitation.

DOI: 10.1021/acsami.6b01031
ACS Appl. Mater. Interfaces 2016, 8, 6423−6430

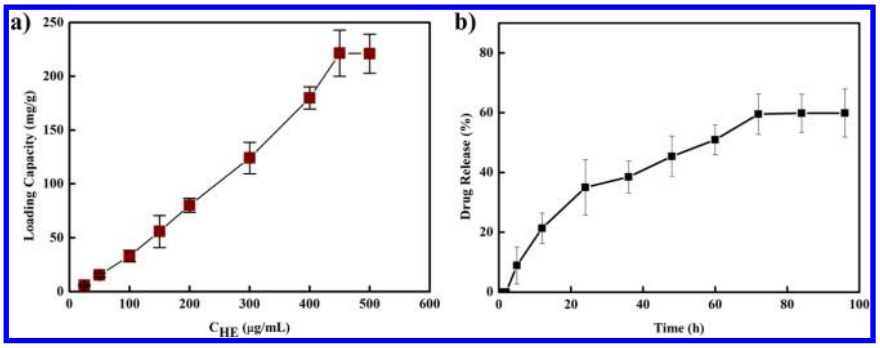

Figure 2. (a) The HE loading capability of FMH NPs at different concentrations of HE in ethanol solution; and (b) cumulative drug release profile of HE from FMH NPs-HE in PBS (100 mM) in vitro.

formation of the second silica layer, the dynamic diameter of NPs increased from 90 to 141 nm, which also indicated the successful synthesis of FMH NPs. In addition, FMH NPs had good dispersity and did not precipitate for several days in media like water, ethanol, DMEM cell culture media (Figure S3). So, it was quite clear that the FMH NPs with good dispersity and appropriate size were suitable for the biological applications. As shown in Figure 1c, the fluorescence intensity of FITC gradually decreased when the silica shell was fabricated step by step. However, the fluorescence intensity of FMH NPs was stronger than FITC@SiO_2@SiO_2 NPs because the silica layer was etched partially by NaOH solution and the transmittance enhanced.[33] Although the fluorescence intensity of FMH NPs was lower than that of pure FITC, it was still strong enough to meet the need of the following experiments. Moreover, the silica shell could protect FITC from photobleaching.[34,35] In summary, FMH NPs displayed strong fluorescence and good photostability (Figure 1c,d), which made them suitable for tracking of intracellular delivery or cellular imaging.

In Figure 1a, FMH NPs show an obvious mesoporous silica shell and a hollow cavity, which can load drugs and small molecular probes. Due to the special structure, they usually have better loading performance than mesoporous silica structures.[36] For our experiments, FMH NPs showed a good HE loading capability of 220 mg/g (Figure 2a). At physiological pH and temperature, about 60 percentage of HE could be released from FMH NPs within 4 days (Figure 2b). Due to the electrostatic interaction between HE (amino group) and FMH NPs (hydroxyl group) as well as hydrophobicity of HE, the release rate was relatively slow.[37] However, the amount of released HE was quite enough for detecting $O_2^{\bullet-}$, because the normal intracellular level of $O_2^{\bullet-}$ was about 0.1 μmmol/L and its concentration could be increased upon oxidative stress.[38] All in all, FMH NPs were excellent nanocarriers to transfer small molecules (especially those insoluble in water or membrane impermeable) into cells for further applications.

Detection of $O_2^{\bullet-}$ Based on FMH NPs-HE. The detection mechanism of this ratiometric sensor was illustrated in Scheme 1. In general, FMH NPs could provide a reference fluorescence signal, and HE, as a recognition molecule toward $O_2^{\bullet-}$, could show quick response to the changes of $O_2^{\bullet-}$ concentration. To verify the possibility of ratiometric measurement of $O_2^{\bullet-}$, we tested the fluorescence spectrum of the FMH NPs and HE signal (Figure 3a). When the sensor was excited by blue light (470 nm), FMH NPs had an emission peak at 518 nm (curve I) and fluorescence was observed for HE (curve II), which could be oxidized by $O_2^{\bullet-}$ to emit stronger fluorescence at 570 nm (curve III). Under the same excitation, the ratiometric

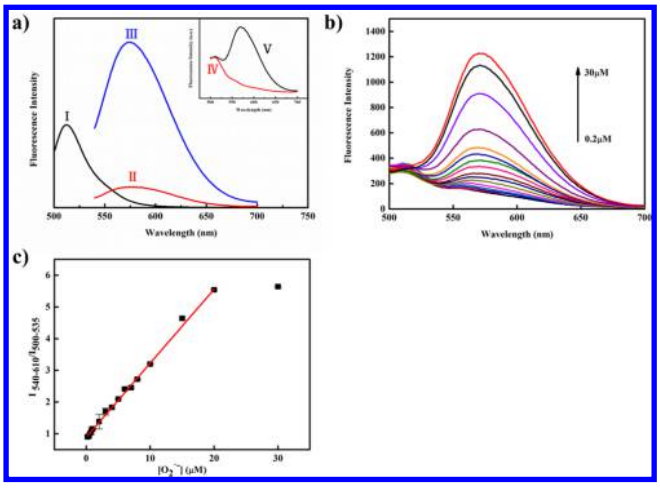

Figure 3. (a) Fluorescence emission spectra (λ_{ex} = 470 nm) of (I) FMH NPs, (II) HE, (III) the products from reaction of HE with $O_2^{\bullet-}$, (IV) nanosensor FMH NPs-HE, and (V) the oxidation product from reaction of nanosensor with $O_2^{\bullet-}$; (b) fluorescence emission spectra of nanosensor with different concentrations of $O_2^{\bullet-}$ upon excitation at 470 nm (0, 0.2, 0.4, 0.6, 0.8, 1, 2, 3, 4, 5, 6, 7, 8, 10, 15, 20, and 30 μM); and (c) plot of $I_{540-610}/I_{500-535}$ as a function of $O_2^{\bullet-}$ concentration obtained with nanosensor in PBS (100 mM).

fluorescent sensor only emitted at 518 nm without $O_2^{\bullet-}$ (curve IV). However, when the sensor was mixed with $O_2^{\bullet-}$, the emission peak of HE oxidation products appeared at 570 nm, but the fluorescence intensity of FMH NPs still remained stable (curve V). Obviously, the fluorescence intensity of HE products was sensitive to the varied amount of $O_2^{\bullet-}$, while that of the FMH NPs was not associated with the concentration of $O_2^{\bullet-}$ and remained almost constant. So, the stable fluorescence intensity of nanoparticles could provide an inner reference for the determination of $O_2^{\bullet-}$ to improve the accuracy and sensitivity. Furthermore, the emission spectrum of FMH NPs was quite narrow and did not overlap with that of HE oxidation products. As a result, FMH NPs and HE were able to constitute an excellent ratiometric fluorescent sensor for detecting $O_2^{\bullet-}$

As expected, the ratiometric fluorescence sensor could effectively detect $O_2^{\bullet-}$ in solution. When the concentration of $O_2^{\bullet-}$ increased from 0 to 30 μM, the fluorescence signal of oxidation products of HE gradually enhanced, while the fluorescence intensity of FMH NPs was almost constant (Figure 3b). In this way, the fluorescence of FMH NPs could act as the reference signal for sensing $O_2^{\bullet-}$, which could be used to correct the environmental errors and improve the detection accuracy.

DOI: 10.1021/acsami.6b01031
ACS Appl. Mater. Interfaces 2016, 8, 6423−6430

It is widely acknowledged that the reaction mechanism between HE and $O_2^{\bullet-}$ is quite complicated. Recent publications have intensive arguments on whether the main product of $O_2^{\bullet-}$ incubated with HE is ethidium (E^+) or not.[39,40] On the whole, 2-hydroxyethidium (2-OH-E^+) are reported to be the main reaction product of $O_2^{\bullet-}$ and HE. When excited at 470 nm, the former emits at 580−600 nm, the latter has an emission at around 570 nm.[41] As shown in Figure 3b, the HE oxidation products emitted at 570 nm, in agreement with the above result. Owing to the fluorescence spectrum overlap of the potential two products and the complex intracellular environment, some reports suggest that it is better to use the integrated intensity for quantification.[9,42] So, we integrated the fluorescence intensity from 540 to 610 nm for HE oxidation products, and used the integrated fluorescence intensity of 500−535 nm for FMH NPs. The intensity ratio of the two emission channels showed good linearity with the concentration of $O_2^{\bullet-}$ ranging from 2.0×10^{-7} to 2.0×10^{-5} M (R^2 = 0.9972), and the detection limit (S/N = 3:1) was calculated to be as low as 80 nM (Figure 3c). Compared with the previous sensors for $O_2^{\bullet-}$ based on X/XO, our sensor achieved a wider linear range and high accuracy, and was suitable for cellular detection.[24,43] In addition, the sensor was also independent of solution pH and kept stable in acid environment, which was beneficial for cellular detection (Figure S4).

Specificity. For cellular applications, the selectivity of the nanosensor to $O_2^{\bullet-}$ was a priority. ROS are composed of many species like H_2O_2, •OH, and $ONOO^-$, which may interfere with the detection of $O_2^{\bullet-}$.[44] In the interference experiment, we recorded the changes of fluorescence intensity ratio ($\Delta I_{540-610}/I_{500-535}$) with the addition of relevant oxidizing materials, and compared it with that of $O_2^{\bullet-}$. In Figure S5, no obvious fluorescence changes were observed in the presence of other ROS (H_2O_2, $^1O_2$, •OH, ROO•, $ONOO^-$) or biologically relevant oxidizing species (NO, NaClO). However, upon adding $O_2^{\bullet-}$ to the analysis system, the fluorescence intensity of HE product was greatly increased. Obviously, the nanosensor exhibited good selectivity toward $O_2^{\bullet-}$ over other ROS or biologically relevant oxidizing species, and could be applied for biosensing and imaging in live cells.

Cytotoxicity of FMH NPs and Nanosensor. In order to study the biocompatibility of the nanosensor, CCK-8 assays were used to evaluate the cytotoxicity of nanocarriers (FMH NPs) and sensors (FMH NPs-HE). The results indicated that HeLa cells still kept high viability after incubating for 24 h either with FMH NPs or nanosensors up to 500 μg/mL (Figure 4). In other words, if the concentration of sensors was not more than 500 μg/mL, then both FMH NPs and the nanosensor had low toxicity to cells, and could be used for cellular sensing and imaging.

Intracellular Biosensing and Bioimaging of $O_2^{\bullet-}$. As described in Scheme 1, the nanosensor with green fluorescence entered into cells, and HE was released and oxidized by $O_2^{\bullet-}$. With an identical excitation, two different colors of fluorescence would be observed, which were ascribed to FMH NPs (green) and HE oxidation products (red), respectively. The overlay of green and red fluorescence images turned out to be yellow. According to the above testing results, the nanosensor showed high sensitivity and selectivity for detection of $O_2^{\bullet-}$ in solution. To further test the ability to detect $O_2^{\bullet-}$ in real complex cellular system, HeLa cells were incubated with 200 μg/mL nanosensors. In Figure 5, the green fluorescence from FMH NPs and red fluorescence from HE oxidation products were both

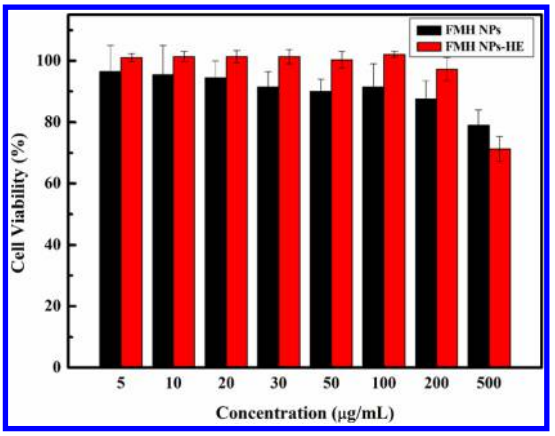

Figure 4. Cell viability of HeLa cells incubated with FMH NPs and nanosensors for 24 h.

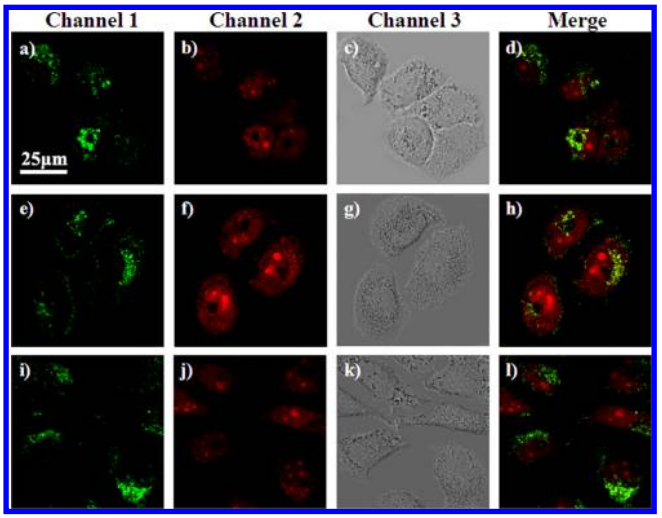

Figure 5. Confocal microscopy images of HeLa cells incubated with 200 μg/mL sensor for 12 h, (a−d) before adding ROSup; (e−h) after stimulated by ROSup for 30 min; (i−l) pretreated with 2 mM GSH for 30 min and then stimulated by ROSup for 30 min. The four columns from left to right were green fluorescence channel images (FMH NPs), red fluorescence channel images (HE oxidation products), bright-field images, overlay images of the first two channels, respectively. The scale bar is 25 μm.

observed in HeLa cells after 12 h incubation. The nonuniform red fluorescence resulted from intrinsic nature of HE. With increased incubation time, red-emitting HE oxidation products would accumulate more in the cell nucleus than in the cytoplasm, and chromatin condensation could also be observed.[40,45] Thus, the nanosensor successfully transported HE to cells to detect $O_2^{\bullet-}$ and still obtained dual-emission in real cellular environment. Besides, the fluorescence intensity of red channel was relatively weak, which indicated a low level of $O_2^{\bullet-}$ in normal condition. Then, ROSup (a positive control of ROS)[46,47] was used to stimulate cells to release more ROS to make cells under oxidative stress. After incubating for 12 h, sensors entered into cells and then ROSup was incubated for another 30 min. The results clearly showed that the intensity of red fluorescence became stronger and the green one still remained unchanged. Thus, from the merged image (Figure 5h), more obvious yellow signal was easily recognized. In addition, to confirm that the stronger intensity resulted from the production of $O_2^{\bullet-}$, GSH, a $O_2^{\bullet-}$ scavenger, was used to

DOI: 10.1021/acsami.6b01031
ACS Appl. Mater. Interfaces 2016, 8, 6423−6430

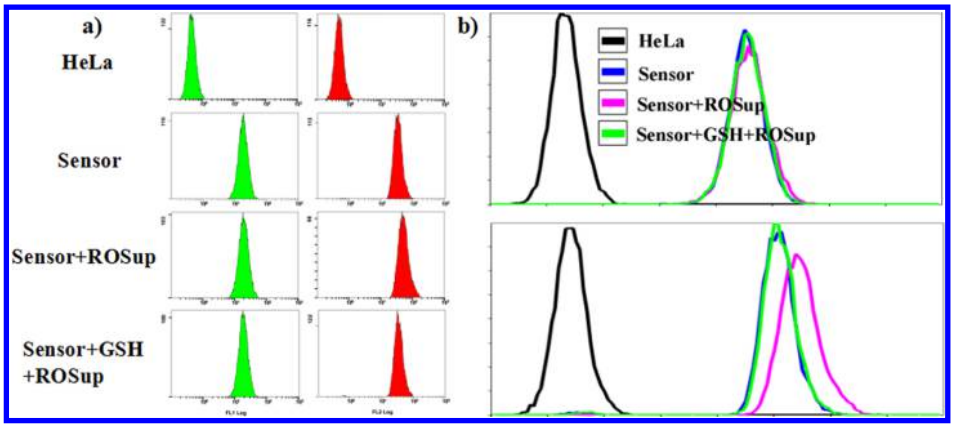

Figure 6. Performance of nanosensors in Flow cytometry analysis. (a) The separate fluorescence histograms of FMH NPs (left) and HE oxidation products (right) came from cells after incubation with nanosensor in presence or absence of ROSup or GSH; and (b) the overlay results of fluorescence histogram of FMH NPs (top) and HE products (bottom) in HeLa cells with as noted treatment.

pretreat the samples before adding ROSup.[9,48] Due to the existence of large amount of GSH, no obvious changes were observed in the red fluorescence channel after the stimulation of the ROSup. In this way, we could make sure that the change of red signal resulted from the increased concentration of $O_2^{\bullet-}$. Just as stated above, the green signal always remained unchanged, while the red channel sensitively changed with stimulation. Besides, due to the enhancement of red fluorescence, the overlay color of the two channels gradually changed from green to yellow. So, we could draw a conclusion that our sensor could obtain dual-emission imaging and realize ratiometric visual recognition of $O_2^{\bullet-}$ in normal condition or under oxidative stress.

The results of confocal image were also examined by Flow cytometry analysis. Compared with the untreated HeLa cells, the fluorescence intensity of the two channels both obviously increased, indicating the successful entry of nanosensors and the detection of $O_2^{\bullet-}$ in live cells (Figure 6a). After interacting with $O_2^{\bullet-}$ induced by ROSup, HE signal was efficiently increased, but not obviously changed after pretreated with GSH (Figure 6b). Moreover, the FMH NPs fluorescence signal still remained constant. So, it could be confirmed that the signal change of nanosensor resulted from the variation of the concentration of $O_2^{\bullet-}$ instead of other effects from environment or light source. In summary, the reference fluorescence signal of FMH NPs could eliminate background interference and improve the detection accuracy. In this way, the ratiometric fluorescence nanosensor provides a reliable method for detecting biological small molecules.

CONCLUSIONS

In this article, we developed a new method to form ratiometric fluorescent sensor, which can be applied to general cases, regardless of the hydrophobicity and membrane-impermeability of probes or difficulty in surface modification. The ratiometric fluorescent nanosensor is composed of nanocarrier doped with reference fluorophore and fluorescent probe for bioactive small molecules. As long as appropriate fluorescent probe and reference fluorophore are selected, the nanosensor could detect a series of bioactive small molecules by ratiometric measurement. As an example, a dual-emission nanosensor was designed for the biosensing and bioimaging of $O_2^{\bullet-}$ in cells, which was composed of FMH NPs, an FITC doped rattle-type silica colloids with strong and stable green fluorescence, and a fluorescent probe toward $O_2^{\bullet-}$, HE. The nanosensor realized ratiometric detection of $O_2^{\bullet-}$ in normal condition or under oxidative stress, with high accuracy and distinguished overlay fluorescence color change. So, this study may provide a simple, accurate, and feasible method for the detection of bioactive small molecules in cells.

ASSOCIATED CONTENT

Supporting Information

The Supporting Information is available free of charge on the ACS Publications website at DOI: 10.1021/acsami.6b01031.

Fluorometric course for the enzymatic reaction of X and XO (Figure S1); TEM image of FITC@SiO_2 NPs (Figure S2); the hydrodynamic size distribution of FMH NPs in cell culture media (Figure S3); effects of pH on fluorescence of the sensor (Figure S4); and the interference experiment data (Figure S5) (PDF)

AUTHOR INFORMATION

Corresponding Authors

*Tel./Fax: +86-25-8359-7204. E-mail: jianglp@nju.edu.cn (L.J.).

*Tel./Fax: +86-25-8359-7204. E-mail: jjzhu@nju.edu.cn (J.-J.Z.).

Author Contributions

‖Y.Z. and J.D. contributed equally to this work.

Notes

The authors declare no competing financial interest.

ACKNOWLEDGMENTS

This work has been supported by Natural Science Foundation of China (Grant Nos. 21475057, 21335004, 81201799), and Program for New Century Excellent Tanlents in University (NCET-12-0256). The authors extend their appreciation to the Deanship of Scientific Research at King Saud University for its funding this Prolific Research Group (PRG-1437-32).

REFERENCES

(1) Mu, B.; Zhang, J. Q.; McNicholas, T. P.; Reuel, N. F.; Kruss, S.; Strano, M. S. Recent Advances in Molecular Recognition Based on Nanoengineered Platforms. *Acc. Chem. Res.* **2014**, *47*, 979−988.

(2) Tavassoli, A.; Hamilton, A. D.; Spring, D. R. Small Molecules in Biology. *Chem. Soc. Rev.* **2011**, *40*, 4269−4270.

DOI: 10.1021/acsami.6b01031
ACS Appl. Mater. Interfaces 2016, 8, 6423−6430

(3) Kumar, S.; Rhim, W. K.; Lim, D. K.; Nam, J. M. Glutathione Dimerization-Based Plasmonic Nanoswitch for Biodetection of Reactive Oxygen and Nitrogen Species. *ACS Nano* **2013**, *7*, 2221−2230.
(4) Lou, Z. R.; Li, P.; Han, K. L. Redox-Responsive Fluorescent Probes with Different Design Strategies. *Acc. Chem. Res.* **2015**, *48*, 1358−1368.
(5) Oushiki, D.; Kojima, H.; Terai, T.; Arita, M.; Hanaoka, K.; Urano, Y.; Nagano, T. Development and Application of a Near-Infrared Fluorescence Probe for Oxidative Stress Based on Differential Reactivity of Linked Cyanine Dyes. *J. Am. Chem. Soc.* **2010**, *132*, 2795−2801.
(6) Liu, H. Q.; Zhang, L.; Chen, J. M.; Zhai, Y. Y.; Zeng, Y. B.; Li, L. A Novel Functional Imidazole Fluorescent Ionic Liquid: Simple and Efficient Fluorescent Probes for Superoxide Anion Radicals. *Anal. Bioanal. Chem.* **2013**, *405*, 9563−9570.
(7) Vonlanthen, M.; Connelly, C. M.; Deiters, A.; Linden, A.; Finney, N. S. Thiourea-Based Fluorescent Chemosensors for Aqueous Metal Ion Detection and Cellular Imaging. *J. Org. Chem.* **2014**, *79*, 6054−6060.
(8) Yun, S. W.; Kang, N. Y.; Park, S. J.; Ha, H. H.; Kim, Y. K.; Lee, J. S.; Chang, Y. T. Diversity Oriented Fluorescence Library Approach (DOFLA) for Live Cell Imaging Probe Development. *Acc. Chem. Res.* **2014**, *47*, 1277−1286.
(9) Gao, X.; Ding, C. Q.; Zhu, A. W.; Tian, Y. Carbon-Dot-Based Ratiometric Fluorescent Probe for Imaging and Biosensing of Superoxide Anion in Live Cells. *Anal. Chem.* **2014**, *86*, 7071−7078.
(10) Ding, C. Q.; Zhu, A. W.; Tian, Y. Functional Surface Engineering of C-Dots for Fluorescent Biosensing and in Vivo Bioimaging. *Acc. Chem. Res.* **2014**, *47*, 20−30.
(11) Kim, J. H.; Ahn, J. H.; Barone, P. W.; Jin, H.; Zhang, J. Q.; Heller, D. A.; Strano, M. S. A Luciferase/Single-Walled Carbon Nanotube Conjugate for Near Infrared Fluorescent Detection of Cellular ATP. *Angew. Chem., Int. Ed.* **2010**, *49*, 1456−1459.
(12) Luo, Z.; Ding, X. W.; Hu, Y.; Wu, S. J.; Xiang, Y.; Zeng, Y. F.; Zhang, B.; Yan, H.; Zhang, H. C.; Zhu, L. L.; Liu, J. J.; Li, J. H.; Cai, K. Y.; Zhao, Y. L. Engineering a Hollow Nanocontainer Platform with Multifunctional Molecular Machines for Tumor-Targeted Therapy in Vitro and in Vivo. *ACS Nano* **2013**, *7*, 10271−10284.
(13) Shi, S. X.; Chen, F.; Cai, W. B. Biomedical Applications of Functionalized Hollow Mesoporous Silica Nanoparticles: Focusing on Molecular Imaging. *Nanomedicine (London, U. K.)* **2013**, *8*, 2027−2039.
(14) Li, N.; Wang, H.; Xue, M.; Chang, C. Y.; Chen, Z. Z.; Zhuo, L. H.; Tang, B. A Highly Selective and Sensitive Nanoprobe for Detection and Imaging of the Superoxide Anion Radical in Living Cells. *Chem. Commun.* **2012**, *48*, 2507−2509.
(15) Li, P.; Zhang, W.; Li, K. X.; Liu, X.; Xiao, H. B.; Zhang, W.; Tang, B. Mitochondria-Targeted Reaction-Based Two-Photon Fluorescent Probe for Imaging of Superoxide Anion in Live Cells and in Vivo. *Anal. Chem.* **2013**, *85*, 9877−9881.
(16) Rastogi, R. P.; Singh, S. P.; Häder, D. P.; Sinha, R. P. Detection of Reactive Oxygen Species (ROS) by the Oxidant-Sensing Probe 20,70-Dichlorodihydrofluorescein Diacetate in the Cyanobacterium Anabaena Variabilis PCC 7937. *Biochem. Biophys. Res. Commun.* **2010**, *397*, 603−607.
(17) Yuan, L.; Lin, W. Y.; Zheng, K. B.; Zhu, S. S. FRET-Based Small-Molecule Fluorescent Probes: Rational Design and Bioimaging Applications. *Acc. Chem. Res.* **2013**, *46*, 1462−1473.
(18) Lan, M. H.; Zhang, J. F.; Chui, Y. S.; Wang, P. F.; Chen, X. F.; Lee, C. S.; Kwong, H. L.; Zhang, W. J. Carbon Nanoparticle-based Ratiometric Fluorescent Sensor for Detecting Mercury Ions in Aqueous Media and Living Cells. *ACS Appl. Mater. Interfaces* **2014**, *6*, 21270−21278.
(19) Shi, W.; Li, X. H.; Ma, H. M. A Tunable Ratiometric pH Sensor Based on Carbon Nanodots for the Quantitative Measurement of the Intracellular pH of Whole Cells. *Angew. Chem., Int. Ed.* **2012**, *51*, 6432−6435.
(20) Shi, W.; Li, X. H.; Ma, H. M. Fluorescent Probes and Nanoparticles for Intracellular Sensing of pH Values. *Methods Appl. Fluoresc.* **2014**, *2*, 042001.
(21) Xu, J. Q.; Liang, J. L.; Li, J.; Yang, W. S. Multicolor Dye-Doped Silica Nanoparticles Independent of FRET. *Langmuir* **2010**, *26*, 15722−15725.
(22) Zheng, F. F.; Zhang, P. H.; Xi, Y.; Chen, J. J.; Li, L. L.; Zhu, J. J. Aptamer/Graphene Quantum Dots Nanocomposite Capped Fluorescent Mesoporous Silica Nanoparticles for Intracellular Drug Delivery and Real-Time Monitoring of Drug Release. *Anal. Chem.* **2015**, *87*, 11739−11745.
(23) Zhang, L. L.; Huang, D. J.; Kondo, M.; Fan, E.; Ji, H. P.; Kou, Y.; Ou, B. X. Novel High-Throughput Assay for Antioxidant Capacity against Superoxide Anion. *J. Agric. Food Chem.* **2009**, *57*, 2661−2667.
(24) Hu, J. J.; Wong, N.-K.; Ye, S.; Chen, X. M.; Lu, M. Y.; Zhao, A. Q.; Guo, Y. H.; Ma, A. C.-H.; Leung, A. Y.-H.; Shen, J. G.; Yang, D. Fluorescent Probe HKSOX-1 for Imaging and Detection of Endogenous Superoxide in Live Cells and In Vivo. *J. Am. Chem. Soc.* **2015**, *137*, 6837−6843.
(25) Maeda, H.; Yamamoto, K.; Nomura, Y.; Kohno, I.; Hafsi, L.; Ueda, N.; Yoshida, S.; Fukuda, M.; Fukuyasu, Y.; Yamauchi, Y.; Itoh, N. A Design of Fluorescent Probes for Superoxide Based on a Nonredox Mechanism. *J. Am. Chem. Soc.* **2005**, *127*, 68−69.
(26) Xu, K. H.; Liu, X.; Tang, B.; Yang, G. W.; Yang, Y.; An, L. G. Design of a Phosphinate-Based Fluorescent Probe for Superoxide Detection in Mouse Peritoneal Macrophages. *Chem. - Eur. J.* **2007**, *13*, 1411−1416.
(27) Li, D. W.; Qin, L. X.; Li, Y.; Nia, R. P.; Long, Y. T.; Chen, H. Y. CdSe/ZnS Quantum Dot-Cytochrome c Bioconjugates for Selective Intracellular $O_2^{\bullet-}$ Sensing. *Chem. Commun.* **2011**, *47*, 8539−8541.
(28) Zielonka, J.; Hardy, M.; Kalyanaraman, B. HPLC Study of Oxidation Products of Hydroethidine in Chemical and Biological Systems: Ramifications in Superoxide Measurements. *Free Radical Biol. Med.* **2009**, *46*, 329−338.
(29) Li, X. Y.; He, J. H. Synthesis of Raspberry-Like SiO_2-TiO_2 Nanoparticles toward Antireflective and Self-Cleaning Coatings. *ACS Appl. Mater. Interfaces* **2013**, *5*, 5282−5290.
(30) Mao, Z. W.; Wan, L.; Hu, L.; Ma, L.; Gao, C. Y. Tat Peptide Mediated Cellular Uptake of SiO_2 Submicron Particles. *Colloids Surf., B* **2010**, *75*, 432−440.
(31) Zhang, Q.; Ge, J. P.; Goebl, J.; Hu, Y. X.; Lu, Z. D.; Yin, Y. D. Rattle-Type Silica Colloidal Particles Prepared by a Surface Protected Etching Process. *Nano Res.* **2009**, *2*, 583−591.
(32) Gun'ko, V. M.; Zarko, V. I.; Voronin, E. F.; Goncharuk, E. V.; Andriyko, L. S.; Guzenko, N. V.; Nosach, L. V.; Janusz, W. Successive Interaction of Pairs of Soluble Organics with Nanosilica in Aqueous Media. *J. Colloid Interface Sci.* **2006**, *300*, 20−32.
(33) Zhang, Q.; Zhang, T. R.; Ge, J. P.; Yin, Y. D. Permeable Silica Shell through Surface-Protected Etching. *Nano Lett.* **2008**, *8*, 2867−2871.
(34) Alberto, G.; Caputo, G.; Viscardi, G. D.; Coluccia, S.; Martra, G. Molecular Engineering of Hybrid Dye−Silica Fluorescent Nanoparticles: Influence of the Dye Structure on the Distribution of Fluorophores and Consequent Photoemission Brightness. *Chem. Mater.* **2012**, *24*, 2792−2801.
(35) Imhof, A.; Megens, M.; Engelberts, J. J.; de Lang, D. T. N.; Sprik, R.; Vos, W. L. Spectroscopy of Fluorescein (FITC) Dyed Colloidal Silica Spheres. *J. Phys. Chem. B* **1999**, *103*, 1408−1415.
(36) Fang, X. L.; Chen, C.; Liu, Z. H.; Liu, P. X.; Zheng, N. F. A Cationic Surfactant Assisted Selective Etching Strategy to Hollow Mesoporous Silica Spheres. *Nanoscale* **2011**, *3*, 1632−1639.
(37) Li, L. L.; Tang, F. Q.; Liu, H. Y.; Liu, T. L.; Hao, N. J.; Chen, D.; Teng, X.; He, J. Q. In Vivo Delivery of Silica Nanorattle Encapsulated Docetaxel for Liver Cancer Therapy with Low Toxicity and High Efficacy. *ACS Nano* **2010**, *4*, 6874−6882.
(38) Yuan, L.; Liu, S. L.; Tu, W. W.; Zhang, Z. S.; Bao, J. C.; Dai, Z. H. Biomimetic Superoxide Dismutase Stabilized by Photopolymerization for Superoxide Anions Biosensing and Cell Monitoring. *Anal. Chem.* **2014**, *86*, 4783−4790.

DOI: 10.1021/acsami.6b01031
ACS Appl. Mater. Interfaces 2016, 8, 6423−6430

(39) Zhao, H. T.; Kalivendi, S. S.; Zhang, H.; Joseph, J.; Nithipatikom, K.; Vásquez -vivar, J.; Kalyanaraman, B. Superoxide Reacts with Hydroethidine but Forms a Fluorescent Product that is Different from Ethidium: Potential Implications in Intracellular Fluorescence Detection of Superoxide. *Free Radical Biol. Med.* **2003**, *34*, 1359−1368.
(40) Lyublinskaya, O. G.; Zenin, V. V.; Shatrova, A. N.; Aksenov, N. D.; Zemelko, V. I.; Domnina, A. P.; Litanyuk, A. P.; Burova, E. B.; Gubarev, S. S.; Negulyaev, Y. A.; Nikolsky, N. N. Intracellular Oxidation of Hydroethidine: Compartmentalization and Cytotoxicity of Oxidation Products. *Free Radical Biol. Med.* **2014**, *75*, 60−68.
(41) Matsuzaki, S.; Szweda, L. I. Inhibition of Complex I by Ca^{2+} Reduces Electron Transport Activity and the Rate of Superoxide Anion Production in Cardiac Submitochondrial Particles. *Biochemistry* **2007**, *46*, 1350−1357.
(42) Patsoukis, N.; Papapostolou, I.; Georgiou, C. D. Interference of Non-specific Peroxidases in the Fluorescence Detection of Superoxide Radical by Hydroethidine Oxidation: a New Assay for H_2O_2. *Anal. Bioanal. Chem.* **2005**, *381*, 1065−1072.
(43) Li, H. M.; Li, Q. L.; Wang, X.; Xu, K. H.; Chen, Z. Z.; Gong, X. C.; Liu, X.; Tong, L. L.; Tang, B. Simultaneous Determination of Superoxide and Hydrogen Peroxide in Macrophage RAW 264.7 Cell Extracts by Microchip Electrophoresis with Laser-Induced Fluorescence Detection. *Anal. Chem.* **2009**, *81*, 2193−2198.
(44) Qu, L. L.; Li, D. W.; Qin, L. X.; Mu, J.; Fossey, J. S.; Long, Y. T. Selective and Sensitive Detection of Intracellular $O_2^{\bullet-}$ Using Au NPs/Cytochrome c as SERS Nanosensors. *Anal. Chem.* **2013**, *85*, 9549−9555.
(45) Saiki, I.; Bucana, C. D.; Tsao, J. Y.; Fidler, I. J. Quantitative Fluorescent Microassay for Identification of Antiproliferative Compounds. *J. Natl. Cancer Inst.* **1986**, *77*, 1235−1240.
(46) Xie, M.; Lu, N. N.; Cheng, S. B.; Wang, X. Y.; Wang, M.; Guo, S.; Wen, C. Y.; Hu, J.; Pang, D. W.; Huang, W. H. Engineered Decomposable Multifunctional Nanobioprobes for Capture and Release of Rare Cancer Cells. *Anal. Chem.* **2014**, *86*, 4618−4626.
(47) Liu, D. D.; Yi, C. Q.; Zhang, D. W.; Zhang, J. C.; Yang, M. S. Inhibition of Proliferation and Differentiation of Mesenchymal Stem Cells by Carboxylated Carbon Nanotubes. *ACS Nano* **2010**, *4*, 2185−2195.
(48) Zhang, W.; Li, P.; Yang, F.; Hu, X. F.; Sun, C. Z.; Zhang, W.; Chen, D. Z.; Tang, B. Dynamic and Reversible Fluorescence Imaging of Superoxide Anion Fluctuations in Live Cells and in Vivo. *J. Am. Chem. Soc.* **2013**, *135*, 14956−14959.

DOI: 10.1021/acsami.6b01031
ACS Appl. Mater. Interfaces 2016, 8, 6423−6430